Chaotic dynamics in coupled resonator sequences

M. Mancinelli,[1,*] M. Borghi,[1] F. Ramiro-Manzano,[1] J. M. Fedeli[2] and L. Pavesi[1]

[1]*Nanoscience Laboratory, Department of Physics, University of Trento, Povo 38123, Trento, Italy*

[2]*CEA, LETI, MINATEC, 17 rue des Martyrs, 38054 Grenoble Cedex 9, France*

**mancinelli@science.unitn.it*

Abstract: Optically induced thermal and free carrier nonlinearities in silicon micro-ring resonator influence their behavior. They can be either deleterious by making them instable and by driving their resonances out of the designed wavelengths, or enabler of different applications. Among the most interesting one, there are optical bistability and self induced oscillations. These lead to all optical logic, signal modulation, optical memories and applications in neural networks. Here, we theoretically and experimentally demonstrate that when many resonators are coupled together, thermal and free carrier nonlinearities induce also chaos. The chaotic dynamics are deeply analyzed using experimentally reconstructed phase space trajectories and the tool of Lyapunov exponents.

© 2014 Optical Society of America

OCIS codes: (130.4815) Optical switching devices; (190.3100) Instabilities and chaos; (230.4555) Coupled resonators.

References and links

1. V. R. Almeida and M. Lipson, "Optical bistability on a silicon chip," Opt. Lett. **29**, 2387–2389 (2004).
2. P. E. Barclay, K. Srinivasan, and O. Painter, "Nonlinear response of silicon photonic crystal microresonators excited via an integrated waveguide and fiber taper," Opt. Express **13**, 801–820 (2005).
3. M. Borselli, T. Johnson, and O. Painter, "Beyond the Rayleigh scattering limit in high-Q silicon microdisks: theory and experiment." Opt. Express **13**, 1515–1530 (2005).
4. Q. Xu and M. Lipson, "All-optical logic based on silicon micro-ring resonators," Opt. Express **15**, 924–929 (2007).
5. T. J. Johnson, M. Borselli, and O. Painter, "Self-induced optical modulation of the transmission through a high-Q silicon microdisk resonator," Opt. Express **14**, 817–831 (2006).
6. G. Priem, P. Dumon, W. Bogaerts, D. Van Thourhout, G. Morthier, and R. Baets, "Optical bistability and pulsating behaviour in silicon-on-insulator ring resonator structures," Opt. Express **13**, 9623–9628 (2005).
7. T. Van Vaerenbergh, M. Fiers, P. Mechet, T. Spuesens, R. Kumar, G. Morthier, B. Schrauwen, J. Dambre, and P. Bienstman, "Cascadable excitability in microrings," Opt. Express **20**, 20292–20308 (2012).
8. T. Van Vaerenbergh, M. Fiers, P. Mechet, T. Spuesens, R. Kumar, G. Mortier, K. Vandoorne, B. Schneider, B. Schrauwen, J. Dambre, and P. Bienstman, "Self-pulsation and excitability mechanism in silicon-on-insulator microrings," in *Asia Communications and Photonics Conference*, J. Opt. Soc. Am. (2012).
9. T. Van Vaerenbergh, M. Fiers, J. Dambre, and P. Bienstman, "Simplified description of self-pulsation and excitability by thermal and free-carrier effects in semiconductor microcavities," Phys. Rev. A **86**, 063808 (2012).
10. A. Armaroli, S. Malaguti, G. Bellanca, S. Trillo, A. de Rossi, and S. Combrié, "Oscillatory dynamics in nanocavities with noninstantaneous kerr response," Phys. Rev. A **84**, 053816 (2011).
11. J. Petráček, Y. Ekşioğlu, and A. Sterkhova, "Simulation of self-pulsing in kerr-nonlinear coupled ring resonators," Opt. Commun. **318**, 147–152 (2014).
12. B. Maes, M. Fiers, and P. Bienstman, "Self-pulsing and chaos in short chains of coupled nonlinear microcavities," Phys. Rev. A **80**, 033805 (2009).

#208088 - $15.00 USD Received 11 Mar 2014; revised 13 May 2014; accepted 21 May 2014; published 5 Jun 2014
(C) 2014 OSA

13. A. Argyris, M. Hamacher, K. Chlouverakis, A. Bogris, and D. Syvridis, "Photonic integrated device for chaos applications in communications," Phys. Rev. Lett. **100**, 194101 (2008).
14. A. Uchida, K. Amano, M. Inoue, K. Hirano, S. Naito, H. Someya, I. Oowada, T. Kurashige, M. Shiki, S. Yoshimori, K. Yoshimura, and P. Davis, "Fast physical random bit generation with chaotic semiconductor lasers," Nature Photon. **2**, 728–732 (2008).
15. A. Yariv, Y. Xu, R. K. Lee, and A. Scherer, "Coupled-resonator optical waveguide: a proposal and analysis," Opt. Lett. **24**, 711–713 (1999).
16. M. Mancinelli, R. Guider, M. Masi, P. Bettotti, M. Vanacharla, J. Fedeli, and L. Pavesi, "Optical characterization of a SCISSOR device," Opt. Express **19**, 13664–13674 (2011).
17. Y. M. Landobasa, S. Darmawan, and M.-K. Chin, "Matrix analysis of 2-d microresonator lattice optical filters," IEEE J. Quantum Electron. **41**, 1410–1418 (2005).
18. M. Mancinelli, PhD Thesis, "Linear and non linear coupling effects in sequence of microresonators," http://eprints-phd.biblio.unitn.it/1050/ (2013).
19. A.A. Kumar, *Fundamentals of Digital Circuits* (Prentice Hall, 2012).
20. F. Takens, "Detecting strange attractors in turbulence," in *Dynamical systems and turbulence, Warwick 1980*, (Springer, 1981), pp. 366–381.
21. J.-P. Eckmann and D. Ruelle, "Ergodic theory of chaos and strange attractors," Reviews of Modern Physics **57**, 617 (1985).
22. M. Cencini, F. Cecconi, and A. Vulpiani, *Chaos: From Simple Models to Complex Systems* (World Scientific Publishing, 2010).
23. S. Chen, L. Zhang, Y. Fei, and T. Cao, "Bistability and self-pulsation phenomena in silicon microring resonators based on nonlinear optical effects," Opt. Express **20**, 7454–7468 (2012).
24. H. A. Haus, *Waves and Fields in Optoelectronics*, vol. 1 (Prentice-Hall 1984).
25. Y. F. Xiao, X. B. Zou, W. Jiang, Y. L. Chen, and G. C. Guo, "Analog to multiple electromagnetically induced transparency in all-optical drop-filter systems," Phys. Rev. A **75**, 063833 (2007).
26. L. F. Shampine and M. W. Reichelt, "The matlab ode suite," SIAM journal on scientific computing **18**, 1–22 (1997).

1. Introduction

The interplay of the diverse optical nonlinearities plays an important role in the response of systems based on optical microcavities. Under continuos wave (CW) excitation, a bistable regime (BR) is established by the dominant nonlinearity [1]. Optical bistability has been extensively studied for the implementation of all-optical switching, logical gates and memories [1–4]. At a certain input power, other competing non-linear mechanisms could emerge inducing an oscillatory time response [5–9]. Several theoretical studies have suggested to exploit self-pulsing (SP) as a route to achieve a chaotic regime (CR) [10–12]. Typically, chaos in photonic circuits is achieved by the inclusion of a cm-size external cavity to a distributed feedback (DFB) III-V laser [13, 14], thus forming a multi-cavity system. An alternative solution exploits Kerr nonlinearities in μm size silicon microresonators. In this way, Armoroli et al. [10] predicted a CR of single resonators with short photon lifetime through an exotic non instantaneous Kerr effect. Nevertheless, in order to achieve such a slow $\chi^{(3)}$ relaxation time (at ps scale), the addition of metals and liquids to the silicon device has been suggested. This limits the resonant cavity feasibility and the industrial manufacturing process, respectively. These technical issues could be faced by employing multi-cavity systems. In fact, there are some theoretical studies that predict a broad CR for passive coupled cavities, like Coupled Resonator Optical Waveguides (CROW) [11] or inline photonic crystal (PhC) nanocavities [12]. However, such models consider the Kerr effect as the only intensity dependent perturbation to the refractive index, neglecting thermal and free carrier ones. This is no longer valid in CW regime, where free carriers and temperature effects dominate over Kerr effects [2]. Therefore, the demonstration either theoretically or experimentally of a silicon-based device showing a CR is still open. In this work, we studied the nonlinear dynamics of Side Coupled Integrated Spaced Sequences of Resonators (SCISSOR) under CW excitation [15, 16]. Compared to the previously reported coupled structures, the SCISSOR configuration is more robust against fabrication defects, and maximizes the intra-cavity optical feedback. This is due to the straight waveguides coupling

#208088 - $15.00 USD Received 11 Mar 2014; revised 13 May 2014; accepted 21 May 2014; published 5 Jun 2014
(C) 2014 OSA

all the resonators, which bypass the imperfections possibly breaking the energy flow along the sequence.

The paper is organized as follows: section 2 presents the device geometry and the experimental setup used to test the SCISSOR response in the frequency and in the time domain. This task is addressed in section 3, where we provide experimental results for the existence of a complex dynamics in the transmitted signal where static, periodic or aperiodic regimes can be observed. Most of the efforts will be devoted to assess the chaotic nature of the aperiodic oscillations. The influence of the input wavelength and of the input power on the onset of chaotic instabilities are studied in section 4. The analysis is completed in section 5, where the role of the device geometry is considered, and a reliable link with chaos is enstablished.

2. Device design and experimental setup

The SCISSOR device has been fabricated on a $200mm$ wafer using $193nm$ DUV lithography. The SOI wafer consists of $220nm$ thick silicon layer laid on top of a $2\mu m$ thick buried oxide (BOX) layer with underlying the silicon substrate. After patterning and etching, a $745nm$ thick silica layer was deposited to form buried single mode channel waveguides of $500 \times 220nm$ cross section. The SCISSOR is composed by a sequence of 8 ring resonators, whose parameters are shown in Fig.1(a). The number of resonators is determined by the amount of power which can be coupled into the Drop port by each ring. With our design parameters, transfer matrix simulations [17] reveal that the input pump power is almost totally depleted after 10 rings, so we fixed the number of resonators to 8. The resonators are designed to have a cavity linewidth of $0.8nm$. The ratio between the resonator separation and its perimeter is 0.5, which ensures the maximum feedback between the cavities [16, 18]. To probe the device spectral response, both in the high power and low power regime, we used the experimental setup sketched in Fig1(b).

A near infrared tunable laser source boosted with an erbium doped fiber amplifier (EDFA) was end-fire coupled to the input waveguide through a lensed optical fiber. The position of the input (output) lensed fiber is controlled with a closed-loop three-axis piezoelectric stages ensuring accurate and stable alignment conditions. TM polarization was used. The signal power was controlled and monitored by using a Variable Optical Attenuator (VOA) and an Optical Spectrum Analyzer (OSA) respectively. In addition, an external $38dB$ fiber optic isolator blocked the light back reflected from the sample facet avoiding spurious effects in the EDFA. The signal polarization was controlled employing two quarter-wave and one half plates placed in an U-bench module before inserting the light into the input waveguide. An InGaAs camera with a $20\times$ objective and $16\times$ zoom lens recorded the radiation scattered out of the surface of the SCISSOR. The output signal from the drop port was collected with another lensed fiber and connected to a detection system, composed by a $10GHz$ photodetector and a $6GHz$ digital oscilloscope. To study the time evolution of the system, a $10GHz$ amplitude modulator was employed to switch off the input signal for a period of $1\mu s$ prior to the signal acquisition. This modulator and the oscilloscope were electrically driven/triggered by an arbitrary function generator. The scattered light from the top of the sample as a function of the input power and wavelength, and the time evolution of the output signal, were remotely acquired by a computer.

3. Dynamic device response

In the spectral domain and at low input powers, the SCISSOR behaves as a bare photonic crystal. The Through spectra consists of a sequence of regions of low transmissivity, where the input signal is resonantly coupled to the ring sequence and is directed to the Drop port [16]. Such wavelength regions are called photonic band gaps (PBG). Since the system is linear, the output power is constant in time. After a certain threshold input power, this is no more true: depending on the input wavelength, a transition from a static output to an unstable one is

#208088 - $15.00 USD Received 11 Mar 2014; revised 13 May 2014; accepted 21 May 2014; published 5 Jun 2014
(C) 2014 OSA

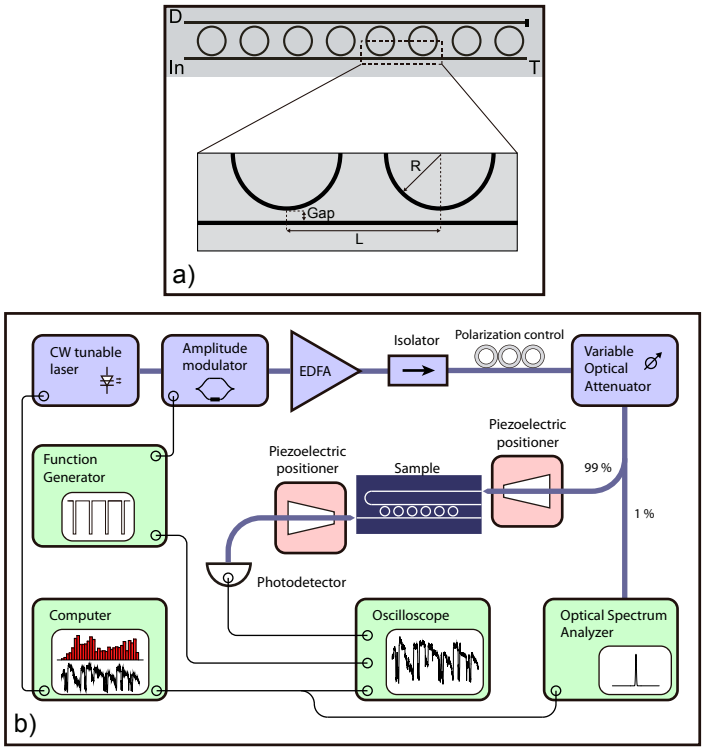

Fig. 1. (a) Sketch of the device geometry. The rings have a nominal radius of $R = 7\ \mu m$ and are separated by a distance $L = 22\mu m$. They are evanescently coupled to the waveguides by means of a $300nm$ gap. The SCISSOR is excited from the Input (In) port. Dropped and transmitted signals are recorded in the Drop (D) and Through (T) ports, respectively. (b) Schematic of the experimental setup.

observed. When this occurs, the Drop(Through) intensity switches from its high(low) constant amplitude to a time varying value. The phenomenon is resonance assisted since it only occurs when the input signal wavelength lies in one of the PBGs. Figure 2 reports some of the observed Drop signal waveforms in the $1542.5 - 1545.5nm$ PBG.

A common feature is the presence of sharp transitions from an high transmission state to a low one and back, creating short time intervals of low intensity separated by transient regions of slowly varying high intensities. Typical time scales are $5ns$ for the sharp features and $70ns$ for the transient ones. The out of plane scattered light signal shown in Fig.2(a) reveals that, during the unstable regime, the signal is localized in a limited number of resonators. The number of resonators to which the input signal efficiently couples is power and wavelength dependent. The complexity of the Drop signal waveforms scales with this number, that we will define as the number of "hot" cavities. The term hot is here used since it corresponds to ring resonators where a high internal energy is accumulated due to the resonant coupling with the input light signal. In Fig.2 it is shown that periodic outputs are observed when a maximum of two resonators become hot. For more hot resonators, the output signal shows complex aperiodic waveforms. The light pattern associated to the waveform in Fig.2(b) shows one of the advantages of using a SCISSOR instead of a CROW or a sequence of inline PhC nanocavities . Even if the two central resonators are off resonance due to fabrication defects, the energy flow along the chain is not interrupted and reaches the last three cavities. In Fig.3 we studied in detail two Drop signal waveforms

#208088 - $15.00 USD Received 11 Mar 2014; revised 13 May 2014; accepted 21 May 2014; published 5 Jun 2014
(C) 2014 OSA

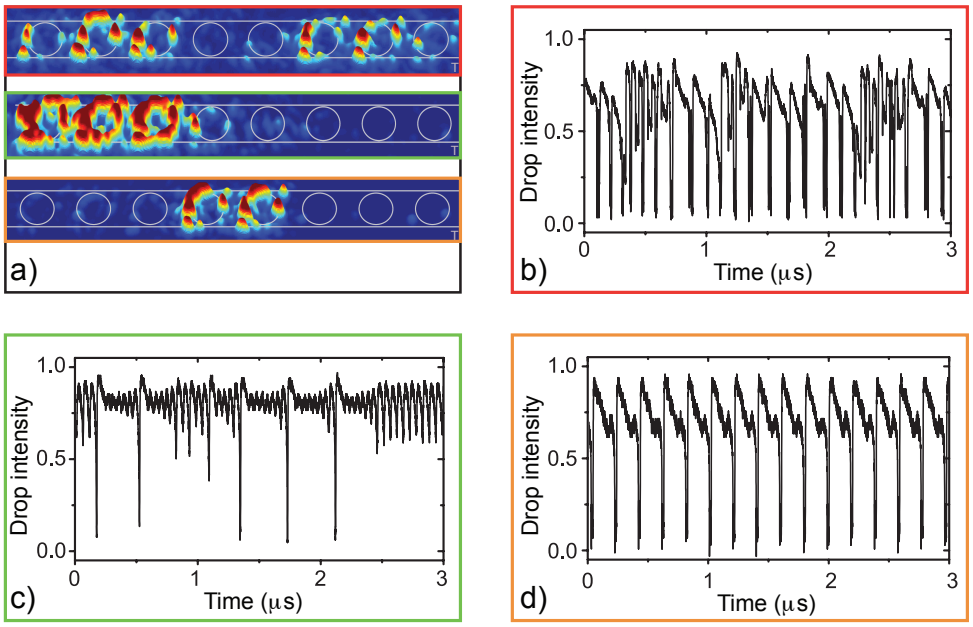

Fig. 2. (a) Top scattered light from the SCISSOR associated to the three waveforms shown in (b-d), respectively. A schematic of the device geometry (white line on the scattering images) illustrates the position of the rings in the chain. (b-d) Drop signal waveforms at different input powers (P_{in}, coupled in the waveguide) and wavelength (λ_p) combinations - (b) $P_{in} = 20mW$ $\lambda_p = 1543.225nm$, (c) $P_{in} = 13mW$ $\lambda_p = 1543.170nm$, (d) $P_{in} = 14.5mW$ $\lambda_p = 1543.990nm$ - showing six (b), three (c) and two (d) hot resonators.

of Fig.2, one periodic (2(d)) and one aperiodic (2(b)). To extract the frequencies with which the sharp transitions recur, the two $50\mu s$ long sequences are converted into binary ones by a digital Schmitt trigger ($10ns$ of hysteresis time) [19]. In Fig.3(a) we reported the histograms of the inverse of the time lags between two subsequent rising edges and their occurrences in the sequences.

The periodic sequence has only one predominant frequency at $15MHz$, while the aperiodic one is characterized by a wider distribution in the $0.5 - 90MHz$ range. The complete lack of regularities in the aperiodic sequence suggests the presence of chaos. If this occurs, two slightly different initial conditions must generate two output signals that lose correlation as the system evolves. The sensitivity to the initial conditions is proven as follows: the input signal of a given wavelength is square wave modulated with a 98% duty cycle. The off duration is nearly $1\mu s$, which is sufficient to let the SCISSOR to relax and thermalize with the environment. The experimental noise (chip temperature and pump intensity fluctuations) makes the initial conditions slightly different every square wave edge front. We recorded the generated sequences in the Drop port and monitored their similarity as a function of time by studying their cross-correlation. Figure 3(b) shows that two periodic sequences with small different initial conditions evolve towards two identical signals that are again periodic and slightly delayed. The case of two aperiodic outputs is different: after few microseconds, the waveforms completely lose their similarity. As shown in Fig.3(d), the cross correlation between the two aperiodic sequences vanishes, meaning that the small perturbations of the initial state are modifying the evolution of the system. To further investigate the presence of chaos, we analyzed the density of points in the phase space. The latter is the N-dimensional space in which the system evolves, where N is

#208088 - $15.00 USD Received 11 Mar 2014; revised 13 May 2014; accepted 21 May 2014; published 5 Jun 2014
(C) 2014 OSA

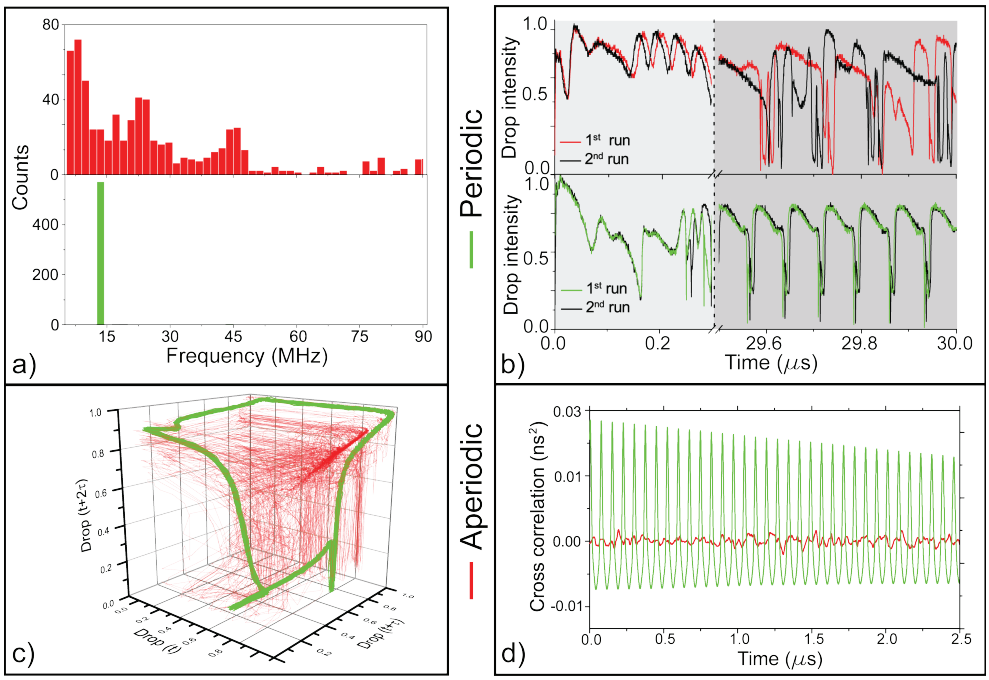

Fig. 3. (a) Frequency distributions of the periodic and the aperiodic Drop signal waveforms shown in Fig.2(d) and in Fig.2(b) respectively. Red bars are for $21mW$ of incident power and $1543.225nm$ of input pump wavelength, while green bars for $21mW$ and $1543.420nm$. (b) Time evolution of two periodic (aperiodic) signals, indicated as run 1 and 2, which start from slightly different initial conditions. Input powers and wavelenght positions are the same as in a. (c) Reconstructed phase spaces of the system for the periodic and the aperiodic outputs in (b). The reconstruction makes use of the Taken's theorem with $m = 2$ and $\tau = 8ns$. (d) Cross correlation between the two periodic (aperiodic) Drop signal waveforms in (b).

the number of its degrees of freedom. At each time, the state of the SCISSOR is identified by a point in that space. The sequence of points in time forms its trajectory. In a chaotic motion, the trajectory is not fixed but explores the phase space in an erratic way. After a long time period this gets densely covered. In our experiment, we do not have access to the complete phase space, since the only measurable quantities are the Through and Drop signal intensities. However, with the help of the Taken's theorem [20], we can construct an equivalent phase space by using m delayed versions of the same Drop(Through) signal. For $m = 1$ we generate a two dimensional space, while for $m = 2$ the space is three dimensional. The reconstructed space preserves the properties of the dynamical system. Figure 3(c) shows a 3D projection of the reconstructed spaces obtained using aperiodic and periodic Drop signals. The periodic sequence (green line) always retraces the same trajectory. The aperiodic sequence has a trajectory that folds on itself several times with no preferential directions and results in a phase space which is dense of points. The high sensitivity to the initial conditions and the dense phase space strongly indicate the presence of chaos.

#208088 - $15.00 USD Received 11 Mar 2014; revised 13 May 2014; accepted 21 May 2014; published 5 Jun 2014
(C) 2014 OSA

4. Influence of the input conditions on the system stability

The transitions between stable, periodic and chaotic regimes are regulated by the input signal wavelength and power. We studied in detail the various regimes by performing a power scan from $5mW$ to $23mW$ (coupled in the waveguide) in the $1542.5-1545nm$ range. The Drop signal is recorded at each combination of input power and wavelength, then the phase space density is calculated using a 2D reconstructed space with $m=1$ and and $\tau=8ns$. The density is defined as the ratio between the visited portion of the phase space and its whole volume. Results are shown in Fig.4(b). High density regions, associated to the most complex and irregular

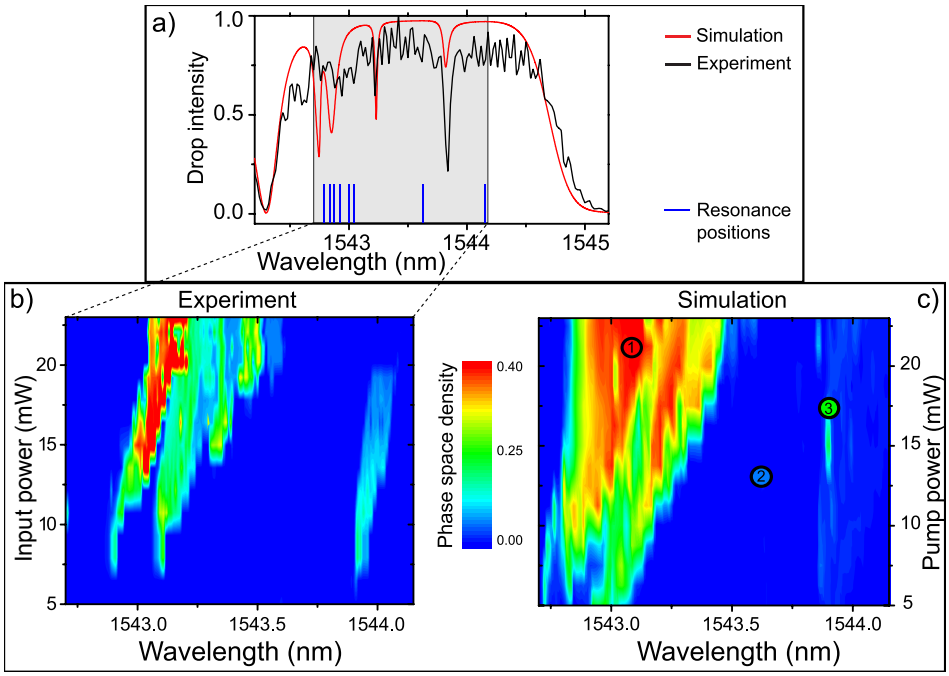

Fig. 4. (a) Experimental (black) and simulated (red) low power ($<mW$) spectral response of the SCISSOR in the $1542.5-1545nm$ range. The resonance positions of each ring in the SCISSOR are indicated with a vertical blue line. (b) Experimental phase space density as a function of the input power and wavelength. (c) Simulated phase space density as a function of the input power and wavelength. Density is computed as in (b) using simulated Drop signals. Colored dots indicate the combinations of input power and wavelength at which the Lyapunov exponents, reported in Fig. 6, are computed. Dots coordinates are ($21.0mW$, $1543.11nm$) for the red one, ($17.8mW$, $1543.91nm$) for the green one and ($13.3mW$, $1543.59nm$) for the blue one.

Drop signal waveforms, are found at high input powers and in the wavelength ranges where the ring resonances lie close together (Fig. 4(a)). The approximate wavelength position of the latter are found by using a transfer matrix code to simulate the SCISSOR's Drop spectra [17]. Transitions towards lower density areas are smooth, indicating that chaotic outputs adiabatically turn to periodic ones before reaching stable states. No oscillations in the Drop signals are observed for input powers below $5mW$. The observed dynamical states and the characteristic time scales are similar to what is found for the self-pulsing in a single silicon microdisk [5], with the important difference that here we do observe also chaotic oscillations due to the SCISSOR structure. The underlying mechanisms leading to instability must, however, be the same.

#208088 - $15.00 USD Received 11 Mar 2014; revised 13 May 2014; accepted 21 May 2014; published 5 Jun 2014
(C) 2014 OSA

The periodic self pulsing of a single cavity arises from a competition between thermal and free carrier nonlinearities [5]. When the pump is tuned near resonance, the field enhancement inside the resonator heats the cavity and generates free carriers through two photon absorption [2]. A temperature increase increases the silicon refractive index, red shifting the resonance wavelength. The generation of free carriers decreases the material refractive index and blue shifts the resonance. At high power, their interplay leads the resonance to oscillate back and forth to the input wavelength, modulating the transmitted intensity. To understand the behavior of our device, we extended the theoretical model in [5] to 8 coupled cavities. The set of dynamical equations governing the cavity interactions is reported in the appendix. Most of the simulation parameters were found by fitting the low power spectral response of Fig.4(a). The accuracy of the model is tested by comparing simulations with experiment at the same input power and wavelength conditions. Figure 5 shows the agreement between a simulated periodic Drop signal waveform and an experimental one. The perodicity of the signal is a fundamental requirement

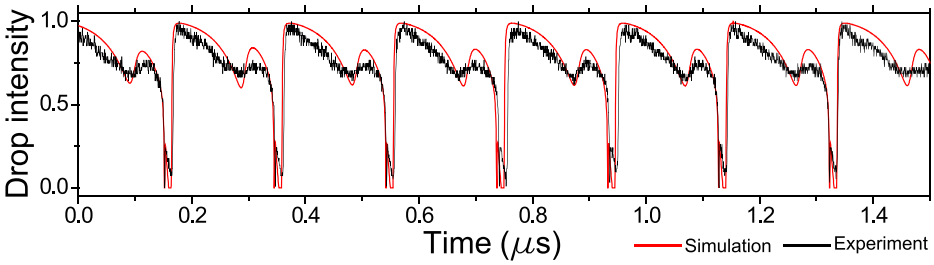

Fig. 5. Comparison between simulation and experiment for an input power of 14.5mW and input wavelength 1543.99nm.

for a correct comparison. In fact, this relaxes the choice of the initial conditions, which are unknown from the experiment (see Fig.3(b)). In this sense, chaotic outputs of a SCISSOR are more unpredictable compared to the non-chaotic outputs of a single resonator, since they depend on a larger number of initial conditions. Using simulated Drop signals, we generated a phase space density diagram (Fig. 4(c)) which is similar to the one of Fig.4(b). High density areas distribution, intensity and shape are again in agreement with the experiment. The model clarifies the role of the input wavelength and power on the system response. The input wavelength selects which rings in the sequence are in resonance, i.e the spectral position of the hot resonators. The increase of the input power induces a resonance oscillation in the hot resonators. As a consequence, the spectral response of the SCISSOR, which depends on the actual position of all the resonances, is time dependent. When many rings have close resonance positions, collective oscillations can be activated at high input powers, which are associated to the localized scattering patterns in Fig.2. The higher the number of hot cavities, the more the spectral response gets distorted and complex waveforms are generated. In some cases, the effect of coupling leads to chaotic. In principle, the presence of fabrication defects is detrimental for the excitation of collective excitations, since it limits the number of cavities having overlapping resonances. However, defects can also induce localized states in which energy is trapped and enhanced, leading to higher nonlinear effects [18].

To prove the existence of a chaotic regime, we calculated the Lyapunov exponents (LE) of the system by integrating the jacobian of Eqs.(1)-(3) (see Appendix) along the simulated trajectories [21]. Positive LE imply ultra-sensitivity to the initial conditions, which is associated to chaotic regimes [22]. LEs are evaluated at three different combinations of power and wavelength, corresponding to regions of low, medium and high phase space density, respectively (colored dots in Fig.4(c)). Figure 6 reports the six Largest Lyapunov Exponents (LLE) in each

#208088 - $15.00 USD Received 11 Mar 2014; revised 13 May 2014; accepted 21 May 2014; published 5 Jun 2014
(C) 2014 OSA

combination.

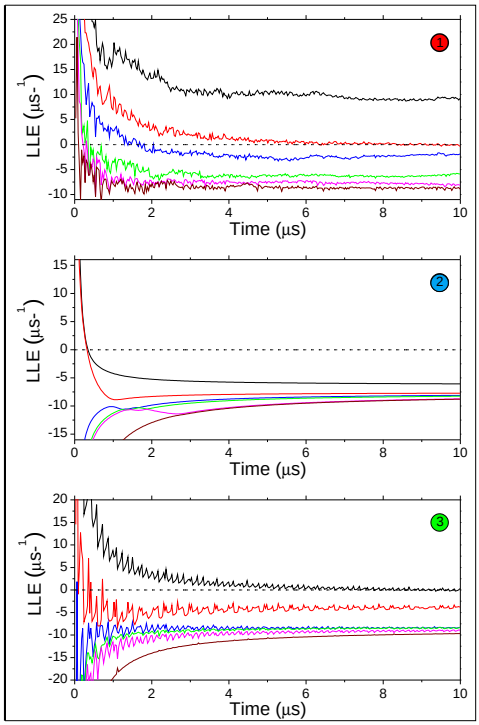

Fig. 6. System stability analysis through Lyapunov Exponents (LE). At each combination of input power and wavelength position, indicated with colored dots in Fig.4(c), the spectrum of Lyapunov exponents of the SCISSOR is computed. As the time evolves, curves in each panel converge to the values of such exponents.Only the largest six LE are plotted in each panel. The Drop signal waveforms (not shown) is constant in the case of the blue dot, periodic for the green one and chaotic for the red one.

The lowest density region has all the LLE lower than zero, which is associated to a stable output. The medium density one has the maximum LE equal to zero, which implies a periodic motion. Finally, the region of highest density admits a positive LE. Theory and experiment are in agreement and prove the existence of a chaotic regime.

5. Sensitivity to device parameters on the onset of chaos

Up to now, we reported on the observation of chaos for a given SCISSOR geometry with 8 resonators. However, a reliable relation between the SCISSOR parameters and chaos would be of much more interest for device engineering. Since we theoretically proved that a two ring system has not positive LE, we simulated a three ring SCISSOR, which allows dealing with a reduced number of degrees of freedom with respect to the 8 cavity system. To further simplify the model, the resonant wavelength of the first ring and the input power are the only variables, as depicted in Fig.7(a).

The investigation of chaos is performed by merging the informations of the phase space density diagram (see e.g Fig.4) together with the ones provided by Lyapunov exponents (see e.g Fig.6) in a single plot (Fig.7(b)). Contour lines, separate regions of positive (chaotic), null (periodic oscillation) and negative (stable state) maximum Lyapunov exponent. We note a power

#208088 - $15.00 USD Received 11 Mar 2014; revised 13 May 2014; accepted 21 May 2014; published 5 Jun 2014
(C) 2014 OSA

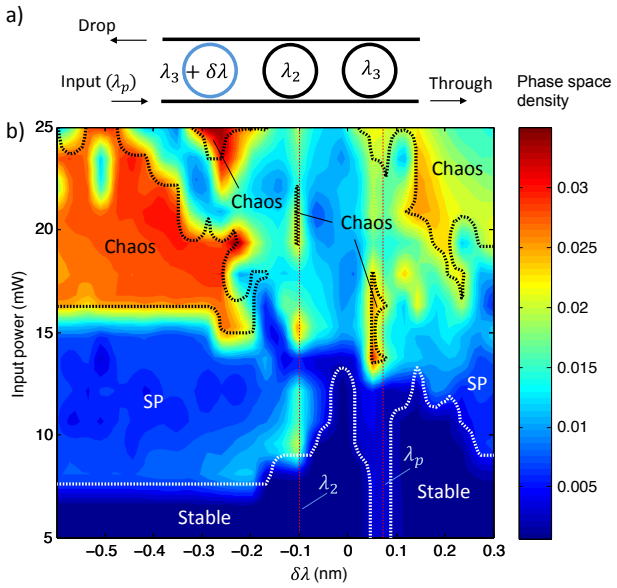

Fig. 7. (a) Sketch of the device geometry. By proceeding from left to right, the three rings have resonance wavelenght $\lambda_1 = \lambda_3 + \delta\lambda$, $\lambda_2 = \lambda_3 - 0.1nm$ and $\lambda_3 = 1542.92nm$ respectively. The input signal wavelength is set to $\lambda_p = \lambda_3 + 0.075nm$. Vertical red lines show the input signal and the central ring resonance wavelengths, respectively.The ratio between the resonator separation and its perimeter is 0.5, which ensures the maximum feedback between the cavities. Each cavity has a linewidth of $0.8nm$. (b) Phase space density plot as a function of the resonance detuning $\delta\lambda$ of the first ring and of the input power. The diagram has been calculated using the same procedure as the one in Fig.4(b). Contour lines separate the regions where the largest Lyapunov exponent turns from negative (labelled Stable) to null (labelled SP, for Self Pulsing regime), null to positive (labelled Chaos) and vice versa.

threshold of $\approx 13mW$ at $\delta\lambda \approx 0.05nm$ for the onset of chaos. Chaos is found at similar powers, both on positive and on negative $\delta\lambda$, where $\delta\lambda$ is the difference between the first and the last cavity resonances. The important difference between these two regions is that the phase space densities, hence the complexity of the output waveforms, are higher at negative detunings. This is not surprising since the chaotic regime requires the self pulsing of resonators, and this is demonstrated to occur only when the input wavelength is red detuned with respect to the cavity resonance [23]. This is due to the fact that at positive detunings, the first cavity works in the optical limiting regime, thus providing a reduced feedback to the others. Furthermore, the power threshold for chaos is much more irregular at positive detunings. Therefore, in spite of the simplicity of the model, a reliable recipe to achieve chaos is found: to obtain a uniform threshold power for a complex chaotic output, all the three cavities must be blue detuned with respect to the input signal wavelength.

6. Conclusions

We reported the experimental observation of chaotic optical signals at the output of a SOI integrated coupled resonator sequence organized in the SCISSOR geometry. Chaos is induced at CW input as a consequence of the complicated interplay between thermal and free carrier nonlinearities which combines to the strong inter-cavity optical feedback. The latter is the new ingredient with respect to single rings where periodic self-pulsing can be only observed. In-

#208088 - $15.00 USD Received 11 Mar 2014; revised 13 May 2014; accepted 21 May 2014; published 5 Jun 2014
(C) 2014 OSA

deed, the coupling among many self-pulsing rings in the sequence allows self-turbulence and hence chaos. We characterized the influence of the device parameters and the input power on the onset of turbulences in the optical domain, by calculating the Lyapunov exponents in a SCISSOR formed by three rings. Our observation of chaos in a SCISSOR could be relevant for the generation of random data sequences, both in the electrical and in the optical domain. In this context, a SCISSOR based random number generator will be conceptually simple and easy to fabricate while preserving the flexibility of silicon photonics, which allows integrating them with other photonic components to realize complex optical functions in a single chip.

7. Appendix: Equations of motion and simulation parameters

Thermal and free carrier nonlinearities are modelled with temporal coupled mode theory. We started from the set of equations in [5] and generalized it to a 8 coupled cavity system. Equations (1)-(5), governing the dynamics of the $i-th$ resonator, have been solved for $i = 1...8$. A description of the terms in Eqs.(1)-(3) is given in Fig.8(a)-(b).

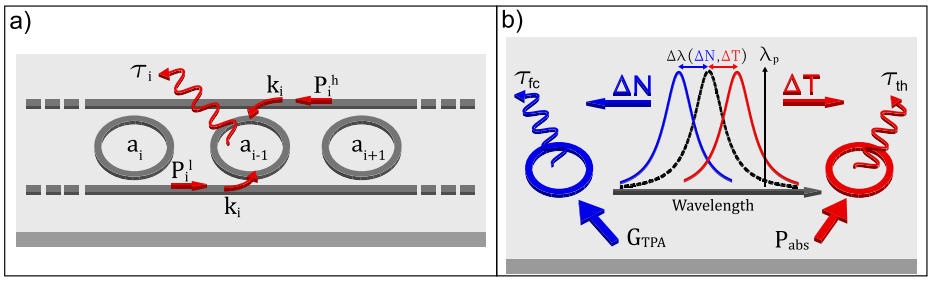

Fig. 8. (a) Cavity interactions: each ring in the chain stores an internal energy $|a_i|^2$. The $i-th$ upper waveguide carries a power P_i^h while the lower one P_i^l. Powers are fed to the cavity with a rate k_i. The cavity loss rate rate $\frac{1}{\tau_i}$ is due to waveguide loading, linear absorption, two photon absorption and free carrier absorption [2]. (b) A differential temperature ΔT is achieved as the result of the balance between the absorbed power P_{abs} and the heat which is dissipated into the external oxide with a rate $\gamma_{th} = \frac{1}{\tau_{th}}$. A differential free carrier population ΔN is obtained by generating electron-hole pairs at a rate G_{TPA} through two photon absorption, and by recombining them with a rate $\gamma_{fc} = \frac{1}{\tau_{fc}}$. Thermal and free carrier effects shift the resonance position λ_0 (black dashed curve in the central inset) by $\Delta\lambda(\Delta T)$ and $\Delta\lambda(\Delta N)$ respectively [2]. The detuning with respect to the input wavelength λ_p is the sum of these shifts.

$$\frac{da_i(t)}{dt} = \left[-j(\omega_p - \omega_{0i}(1+\Delta\omega(\Delta T_i(t)) + \Delta\omega(\Delta N_i(t))) - \frac{1}{\tau_i(a_i(t))}\right] a_i(t) + j\sqrt{k_i}(P_i^l(t) + P_i^h(t)) \quad (1)$$

$$\frac{d\Delta T_i(t)}{dt} = -\gamma_{fh}\Delta T_i(t) + P_{abs,i}(a_i(t), \Delta N_i(t)) \quad (2)$$

$$\frac{d\Delta N_i(t)}{dt} = -\gamma_{fc}\Delta N_i(t) + G_{TPA,i}(a_i(t)) \quad (3)$$

$$P_i^l(t) = e^{-j\phi_L}\left(P_{i-1}^l(t) + j\sqrt{k_{i-1}}a_{i-1}(t)\right) \quad (4)$$

$$P_i^h(t) = e^{-j\phi_L}\left(P_{i+1}^h(t) + j\sqrt{k_{i+1}}a_{i+1}(t)\right) \quad (5)$$

#208088 - $15.00 USD Received 11 Mar 2014; revised 13 May 2014; accepted 21 May 2014; published 5 Jun 2014
(C) 2014 OSA

The term ϕ_L at the exponential in Eqs.(4)-(5) is the phase accumulated by the signal during the propagation in the straight waveguide sections separating two neighboring resonators. The propagation and bending lossess have been set to $2dB/cm$ [16]. The coupling term $j\sqrt{k_i}(P_i^l(t)+P_i^h(t))$ can be deduced from energy conservation [24, 25]. The model consider a strictly unidirectional propagation, backward waves generated by surface roughness have not been considered.

Table 1. Values of the simulation parameters. The design value of the resonator radius R_0 is perturbed by a quantity ΔR_i because of fabrication errors.

Parameter	Value			
$\lambda_{0i}=\frac{2\pi c}{\omega_{0i}}$	i		i	
	1	$1543.00nm$	5	$1544.21nm$
	2	$1542.92nm$	6	$1542.83nm$
	3	$1542.80nm$	7	$1542.79nm$
	4	$1543.67nm$	8	$1543.06nm$
$k_i=\kappa^2\cdot\frac{2\pi(R_0+\Delta R_i)n_g}{c}$	$\kappa^2=0.12$, $n_g=3.8051$, $R_0=7\mu m$			
ΔR_i	i		i	
	1	$0.726nm$	5	$12.060nm$
	2	$-0.015nm$	6	$-0.822nm$
	3	$-1.080nm$	7	$-1.237nm$
	4	$7.000nm$	8	$1.311nm$
$\phi_L=\frac{\omega_{0i}}{c}n_{eff}L$	$n_{eff}=1.78$, $L=22.03\mu m$			
$\gamma_{th}=\frac{1}{\tau_{th}}$	$7.2\mu s^{-1}$			
$\gamma_{fc}=\frac{1}{\tau_{fc}}$	$220\mu s^{-1}$			

The set of equations has been integrated using a variable order solver [26]. Values of ω_{0i}, k_i and ϕ_L for $i=1...8$ have been extracted by fitting the experimental spectral response in the $1542.5-1545nm$ range (Fig.3(a)) using a transfer matrix method [17]. Values of the thermal and free carrier decay rates γ_{TH} and γ_{FC} have been extracted by fitting the modulated Drop signal of a single cavity having the same geometry as the ones composing the SCISSOR. The list of extracted parameters is given in Table 1. The expressions for P_{abs_i}, G_{TPA_i} and τ_i are directly taken from [5] and subsequently adapted to our device geometry.

#208088 - $15.00 USD Received 11 Mar 2014; revised 13 May 2014; accepted 21 May 2014; published 5 Jun 2014
(C) 2014 OSA